Exp Fluids (2008) 45:927–941
DOI 10.1007/s00348-008-0511-7

RESEARCH ARTICLE

Effect of predictor–corrector filtering on the stability and spatial resolution of iterative PIV interrogation

F. F. J. Schrijer · F. Scarano

Received: 16 December 2005 / Revised: 21 April 2008 / Accepted: 23 April 2008 / Published online: 20 May 2008

Abstract The stability and resolution of iterative PIV image analysis methods is investigated. The study focuses on the effects of stabilization by means of spatial filtering when implemented into the iterative process. Two filtering approaches are studied: predictor and corrector filtering respectively. A family of convolution filters is proposed, which allows to vary the filtering strength in a systematic way and primarily affects the system stability and to a smaller extent its spatial response. A critical value for the filter parameter is identified which guarantees the stability of the iterative process. A theoretical analysis is provided that determines the asymptotic properties of the iterative method with varying filter parameters. The study is completed with a numerical assessment and concludes with an application to real experiments, showing the consequence of an incorrect implementation of the iterative scheme under experimental conditions.

1 Introduction

PIV iterative image interrogation methods are nowadays a common adopted choice due to the significantly augmented measurement capabilities. The computer power currently available at affordable costs allows researchers to perform multiple interrogation steps for a single recording within the minute. The most important advantages of multi-grid techniques are the increase of dynamic range eliminating the constraint of the ¼ rule for the in-plane motion (Keane and Adrian 1993) and an increased measurement precision (Soria 1996; Westerweel et al. 1997; Scarano and Riethmuller 1999). The introduction of the iterative sub-pixel window shift technique (Lecordier 1997) showed that an important improvement could be obtained also in terms of measurement sub pixel precision. The iterative window deformation method (Huang et al. 1993; Jambunathan et al. 1995) opened the way to the development of more sophisticated algorithms able to cope with flows exhibiting a large velocity gradient minimizing correlation peak broadening. The most important improvement brought to the technique was in terms of the velocity gradient dynamic range (Fincham and Delerce 2000; Scarano and Riethmuller 2000a). However, the properties of the iterative interrogation process, expressed as the stability and the spatial resolution of the converged results were not well understood. Consequently the interrogation process required a user-determined criterion to terminate the analysis. Nogueira et al. (1999) reported about the possible unstable behaviour of iterative cross-correlation interrogation when performed with the image deformation technique and proposed a strategy how to avoid the instability. During the worldwide PIV challenge II (Stanislas et al. 2005), the issue of the iterative image deformation method stability was repeatedly raised due to the large number of researchers and system manufacturers adopting iterative interrogation methods with implementations varying among the different developers. The worldwide PIV challenge III showed that nowadays the image deformation technique could be considered as part of the standard interrogation method.

This discussion motivates the authors to investigate the stability (Scarano 2004) and the spatial resolution of iterative methods based on cross-correlation analysis and image deformation from a fundamental standpoint. The work focuses in particular on the effect of spatial filtering

F. F. J. Schrijer (✉) · F. Scarano
Department of Aerospace Engineering,
Delft University of Technology, Kluyverweg 1,
2629 HS Delft, The Netherlands
e-mail: f.f.j.schrijer@tudelft.nl

of the velocity distribution to prevent the amplification of velocity fluctuations at specific wavelengths during the iterative interrogation. This procedure is commonly adopted in the research community (Lecordier and Trinité 2003; Scarano 2004), therefore the low-pass filtering procedure and filter properties are investigated to establish a better knowledge when designing and developing iterative interrogation algorithms.

The first part of the paper is devoted to the theoretical analysis of the iterative process corresponding to cross-correlation predictor–corrector interrogation. The model including the filtering procedure is then assessed by means of computer simulated PIV recordings with known sinusoidal displacement properties.

The theoretical and numerical investigation focuses on one-dimensional signals representing a generic flow situation where a spatial wavelength dominates in one direction, for example shear layers or shock waves. Flow situations where the spatial wavelengths are of the same order in all directions (isotropic turbulence, vortices) are studied by means of two-dimensional signals.

The results are verified with the application to a turbulent flow over a backward facing step. The tests performed under experimental conditions allows to state how much can be inferred from numerical assessment when noise terms cannot be neglected (out-of-plane motion, background light, CCD noise).

2 Iterative interrogation with image deformation

The iterative analysis of PIV recordings can be schematically described as being composed of two parts (Scarano and Schrijer 2005):

(1) *Multi-grid analysis* where the interrogation window size is progressively decreased. This process eliminates the ¼ rule constraint and it usually ends when the required window size has been reached.
(2) *Iterative analysis* at a fixed window size (and grid spacing). This process allows to further improve the accuracy of the image deformation (Nogueira et al. 1999; Scarano 2000) and to a certain extent allows to enhance the spatial resolution of the measurement.

The present investigation is concerned solely with the iterative analysis. In its essence the process can be described by a predictor–corrector loop as schematically represented in Fig. 1. The iterative equation in its simplest form reads as:

$$\vec{V}^{k+1} = \vec{V}^{k} + \vec{C}^{k+1}, \tag{1}$$

where $\boldsymbol{V^k}$ indicates the velocity field resulting from the evaluation at the kth iteration and is used as predictor for the following iteration. The correction term $\boldsymbol{C^k} = (c_u, c_v)$ is the vector determined by cross-correlating the deformed images: $\vec{C}^{k} = I_a^k \otimes I_b^k$. The deformed images are obtained from the original images I_a, I_b according to the relation:

$$\begin{aligned} I_a^k(x,y) &= I_a(x - u_d^k/2, y - v_d^k/2) \\ I_b^k(x,y) &= I_b(x + u_d^k/2, y + v_d^k/2). \end{aligned} \tag{2}$$

here u_d,v_d is the image deformation displacement at location (x,y) commonly obtained interpolating the predictor displacement $\boldsymbol{V^k}$ onto a pixel grid. The most common choice for the displacement interpolation is bi-linear (Huang et al. 1993; Jambunathan et al. 1995; Scarano and Riethmuller 2000a) which is also used in the current investigation. Higher order functions have also been considered (Fincham and Delerce 2000; Lecordier and Trinité 2003), which may in principle improve the accuracy of image deformation. In all cases where sub-pixel image transformation is required (sub-pixel window shift and/or window deformation), the images have to be interpolated for re-sampling at non-integer pixel positions. The topic is extensively discussed by Astarita and Cardone (2005), who conclude that high-order interpolators are necessary to achieve higher accuracy, although high noise levels may reduce the relative improvements obtained for high order interpolators (Astarita 2006). In the current study image interpolation is performed using a sinc interpolation with an 11 × 11 pixel kernel size.

The approach as described in the block diagram of Fig. 1 may appear very logical and its simplicity makes it straightforward to implement, which probably justifies why it has been broadly adopted in the PIV community. However it will be discussed why this approach is incomplete and may lead to inaccurate results.

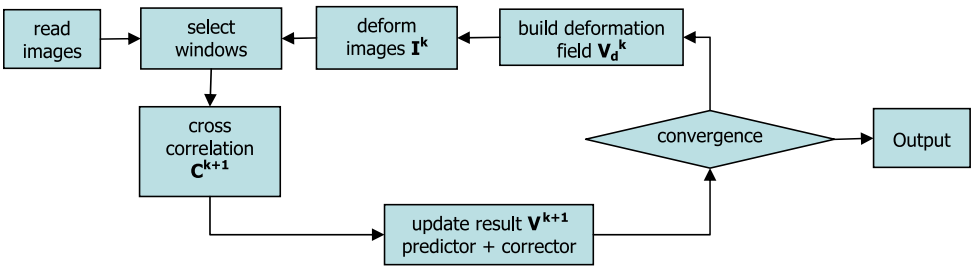

Fig. 1 Block diagram of the iterative image deformation interrogation method

2.1 Theoretical stability analysis

It has been shown (Nogueira et al. 1999; Scarano 2004; Astarita 2006) that the iterative process is intrinsically unstable and the result may diverge unless the image processing is interrupted at an early stage. The instability can be investigated by looking at the nature of the cross correlation process. The particle displacement obtained by image cross correlation is shown to be similar in applying a moving average filter to the exact displacement field when the correlation window contains sufficient particles (Scarano and Riethmuller 2000a). Therefore the frequency response of the cross correlation process is equivalent to that of a moving average filter having a kernel size equal to the window size. This frequency response is given by the sinc function, which is depicted Fig. 2.

Here l^* is the normalized window size, which is the linear window size divided by the signal wavelength $l^* = WS/\lambda$. When $l^* \to 0$, the window size is small with respect to the signal wavelength. Conversely when $l^* \to \infty$, the window size is large with respect to the signal wavelength. The response function becomes negative for certain values of l^*. Applying this observation to the cross correlation process means that at certain wavelength intervals, having a negative response, the cross correlation result will be opposite to the actual displacement. For an iterative approach this means that the process is potentially unstable and may diverge at these specific wavelengths. Therefore when regarding the frequency response of the conventional single-step PIV cross correlation process, the instability in the process is produced at intervals having negative values (Nogueira et al. 1999) which are located between 1 and 2, 3 and 4 and so on.

As mentioned before, the frequency response of single-step cross-correlation analysis is equivalent to the sinc function for which the largest negative value is found close to $l^* = 1.5$. Therefore in a PIV process, wavelengths 2/3 of the window size will be amplified provided the employed overlap factor is larger than 50% so that the wavelength can be represented (although affected by modulation). This can be illustrated by analysing a synthetic PIV recording where the two exposures have a zero relative displacement. A small amount of uncorrelated noise (0.4% pixel noise) is added. The iterative PIV interrogation returns after 20 iterations the result depicted in Fig. 3. Here the most amplified waves are clearly visible and the wavelength coincides with 2/3 of the interrogation window size ($l^* = 1.5$).

This aspect has already been studied and different solutions are possible. Image weighting functions such as Gaussian or LFC (Nogueira et al. 1999, 2001; Astarita 2007) may reduce or eliminate the mentioned instability by means of eliminating the sinc negative sidelobes, however at the cost of lower effective image number density. This is counterbalanced using relatively large correlation kernels (e.g. 64 × 64) but still keeping a small distance between adjacent windows. In a recent study from Nogueira et al. (2005) it is stated that large windows are needed to achieve an accurate representation of the weighting function on the discrete pixel grid. The resulting overlap factor implies that a large number of computations have to be performed.

A comparison of the image weighting approach with the vector data filtering discussed in this paper was performed in Schrijer and Scarano (2006). Here it was found that the modulation as well as rms errors were reduced, however at the cost of a considerable increase of computational time.

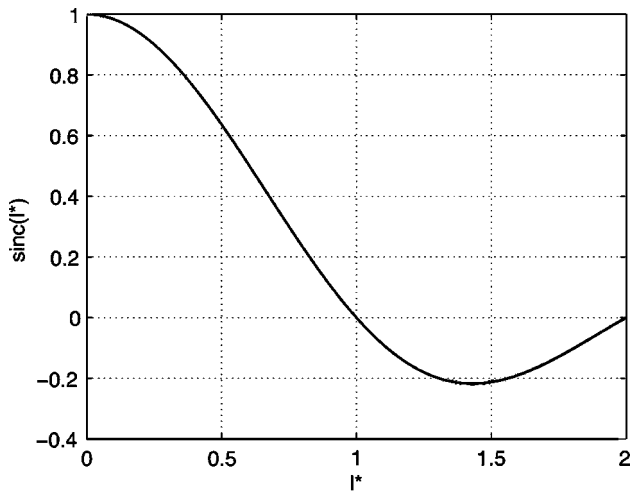

Fig. 2 Cross correlation frequency response: sinc function

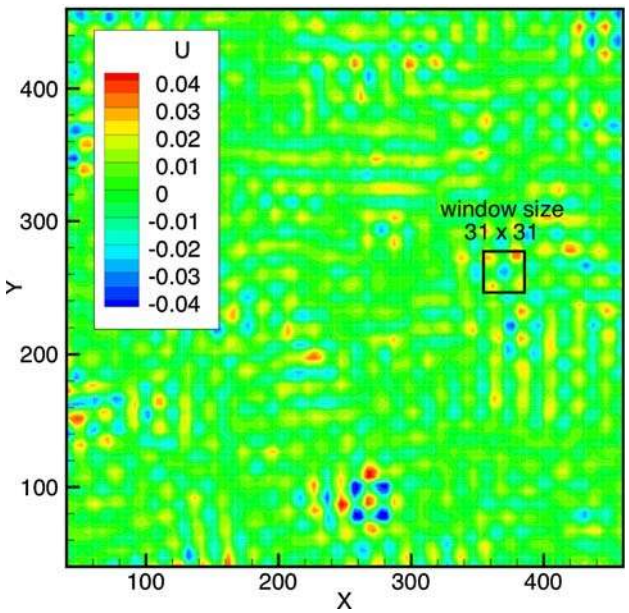

Fig. 3 Iterative PIV result after 20 iterations for a zero displacement velocity field (0.4% pixel noise)

3 Stabilization through spatial filtering

Another approach consists in the analysis by cross correlation without window weighting, however applying a spatial filter (low-pass) to the velocity field. The interesting aspect of this approach resides in the limited computational effort. The velocity field spatial distribution can be filtered at several points within the iterative process (Fig. 4), where the different choices yield a specific behaviour of the iterative method.

The filtering process can be described as a convolution operation applied to the pixel-grid velocity field (either $\boldsymbol{V}^{\boldsymbol{k}}$ or $\boldsymbol{C}^{\boldsymbol{k}}$). It can be mathematically represented as:

$$\vec{F}(\vec{V}) = \iint_{W} f(\xi,\ \eta)\vec{V}(\xi - x,\ \eta - y)\mathrm{d}\xi\mathrm{d}\eta. \tag{3}$$

The operation returns a filtered version of the velocity vector field $\boldsymbol{F}(\boldsymbol{V})$. Where f is the filter and W is the linear filter kernel size.

It will be shown that the purpose of the filter is to prevent the growth of velocity fluctuations at unstable wavelengths. It should be kept in mind that excessive filtering would result in a highly stable process, however this will be at the cost of reduced spatial resolution. Conversely, no or insufficient filtering will not damp the instability growth with poor convergence of the iterative process and a low accuracy measurement. Therefore the influence of the filter properties such as size and shape on the stability and spatial resolution should be carefully assessed.

In the current study the predictor filtering and corrector filtering approaches are investigated, both strategies are further outlined in the following sections.

3.1 Predictor filtering approach

As the name already suggests the velocity predictor is filtered in the iterative loop before image deformation, as shown in the block diagram of Fig. 4. The iterative equation in this case can be written as:

$$\vec{V}^{k+1} = \vec{F}(\vec{V}^{k}) + \vec{C}^{k}. \tag{4}$$

Introducing the spatial response of the chosen convolution filter r_{f}, the exact value of the particle images displacement V_0 and the characteristic response of the filter used for the image weighting r_{c} [which is equal to sinc(l*) for a top-hat window] the iterative equation can be further reformulated as:

$$\vec{V}^{k+1} = r_{\mathrm{f}} \cdot \vec{V}^{k} + r_{\mathrm{c}} \cdot (\vec{V}_0 - r_{\mathrm{f}} \cdot \vec{V}^{k}). \tag{5}$$

3.2 Corrector filtering approach

When applying corrector filtering the direct result of cross correlation is subject to the filter and the iterative equation can be written as:

$$\vec{V}^{k+1} = \vec{V}^{k} + \vec{F}(\vec{C}^{k}). \tag{6}$$

Following the approach similar to predictor filtering the iterative equation becomes:

$$\vec{V}^{k+1} = \vec{V}^{k} + r_{\mathrm{c}} \cdot r_{\mathrm{f}} \cdot (\vec{V}_0 - \vec{V}^{k}). \tag{7}$$

Equations (5) and (7) for predictor and corrector filtering are analogous to those proposed by Nogueira et al. (1999, 2005) except for the introduction of the filtering term r_{f}.

It may be anticipated that the filter has a larger influence when it is implemented in the predictor mode since it directly acts on the previously measured displacement field while the corrector filter only acts on the update term and thus affects the result indirectly.

3.3 Parametric filter approach

To avoid a multi-parametric analysis of the system behaviour in relation to the filter properties a family of filters is introduced having a fixed kernel length. The filter shape depends on a single parameter chosen such that the entire range of filtering possibilities, from the Dirac delta function to the moving average (MA) can be covered, whereas the filter kernel size is kept constant. However, the filter shape might not be the optimal one for a given filtering strength.

The one-dimensional formulation of the filter is described by the following equation:

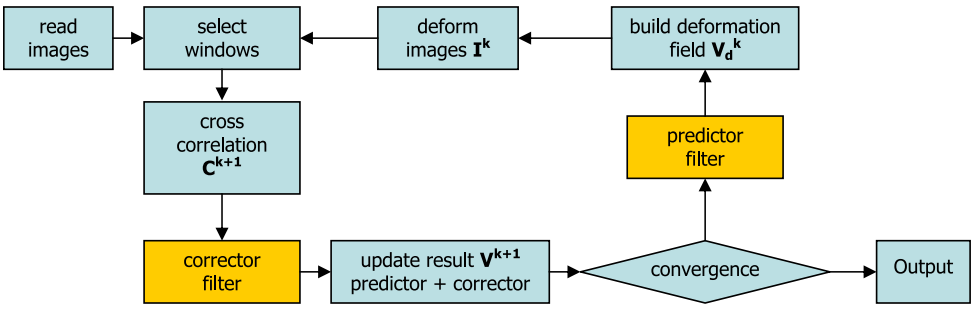

Fig. 4 Block diagram of the iterative image deformation interrogation method with filtered predictor and filtered corrector options

$$f_{1D}(\xi) = C_1\left[\left(\frac{l}{2}\right)^z - |\xi|^z\right], \tag{8}$$

where C_1 normalizes the filter integral to unit value. The kernel window size is given by l and it has been chosen equal to the PIV interrogation window size. When $z \to 0$ the filter approximates a Dirac delta function, which corresponds to the case of no filtering. For increasing values of the parameter z the filter shape becomes fuller, as shown in Fig. 5 left. When $z \to \infty$, the function approximates a top-hat filter with the same dimension as the interrogation window, although the filter is still equal to 0 at the edges. At $z = 1$ the filter represents a triangular function. The filtering strength therefore increases with z and it is expected that for higher values of z the filter becomes increasingly effective in damping instabilities, however at the cost of a lower spatial resolution. The corresponding two-dimensional filter is given by the following expression (see Fig. 5 right):

$$f_{2D}(\xi,\eta) = \begin{cases} C_2\left[\left(\frac{l}{2}\right)^z - |\xi|^z\right] & \text{for } |\xi| \geq |\eta| \\ C_2\left[\left(\frac{l}{2}\right)^z - |\eta|^z\right] & \text{for } |\xi| < |\eta| \end{cases} \tag{9}$$

with C_2 being the normalization coefficient.

As stated in the "Introduction", the two-dimensional signals are representative of flow fields with spatial fluctuations along both directions where no direction dominates. To limit the number of free variables in the present study, two-dimensional cases are considered with signals having the same wavelength in both x and y directions $\lambda_x = \lambda_y = \lambda$.

The filters used in the theoretical approach are introduced as continuous functions therefore eliminating the error due to spatial discretization. The spatial response r_f of the one-dimensional filter is given in Fig. 6 left. Repeating once more the definition of the normalized window size l^* (spatial frequency) as the ratio of the filter window size (which is equal to the PIV interrogation window size) and the velocity spatial distribution wavelength (WS/λ). Clearly for $z \to \infty$, r_f approaches the sinc(l^*) function. As z is decreased, the modulation decreases. When $z \to 0$, the modulation becomes constant at a value of 1 ($r_f \to 1$) approaching the ideal impulse response (no modulation). The two-dimensional filter spatial response (Fig. 6 right) has similar characteristics to the one-dimensional. Since the wavelengths are equal in x and y directions, the filter spatial response only depends on l^*. The modulation increases with z and approaches 1 for $z \to 0$.

Subsequently the filter spatial response is used to obtain a theoretical estimate of the effect of the parameter z on the asymptotic properties of the iterative process. The analysis focuses primarily upon the stability and spatial resolution of the iterative process and is used to gain insight into the effects of the filtering on the iterative process.

3.4 Non-linear filtering approach

The additional case of a non-linear filter is investigated. It is implemented in the predictor step. The iterative equation reads as:

$$\vec{V}^{k+1} = \vec{F}_{\text{regr}}\left(\vec{V}^k\right) + r_c \cdot \left[\vec{V}_0 - \vec{F}_{\text{regr}}\left(\vec{V}^k\right)\right] \tag{10}$$

where $\boldsymbol{F}_{\text{regr}}(\boldsymbol{V}^k)$ represents the velocity field filtered by means of a second order two-dimensional least squares regression with a kernel size l equal to the interrogation window size WS. The advantage of this filter is a favourable combination of noise reduction behaviour and low spatial modulation. Due to the non-linearity of the filter it is not possible to infer its spatial response, therefore it is not included into the theoretical discussion. However it will be compared to the linear filters in the numerical and experimental assessment.

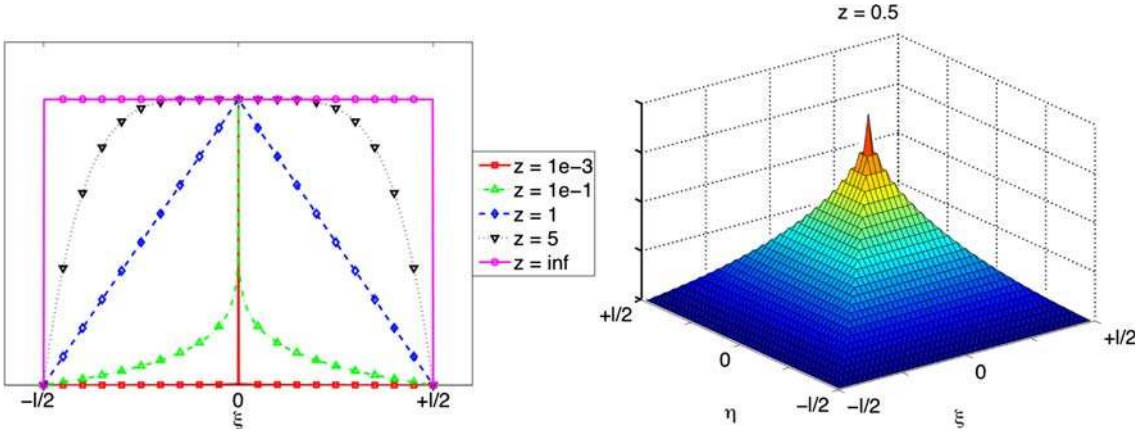

Fig. 5 Convolution filter family, one-dimensional (*left*) without normalization coefficients and two-dimensional (*right*)

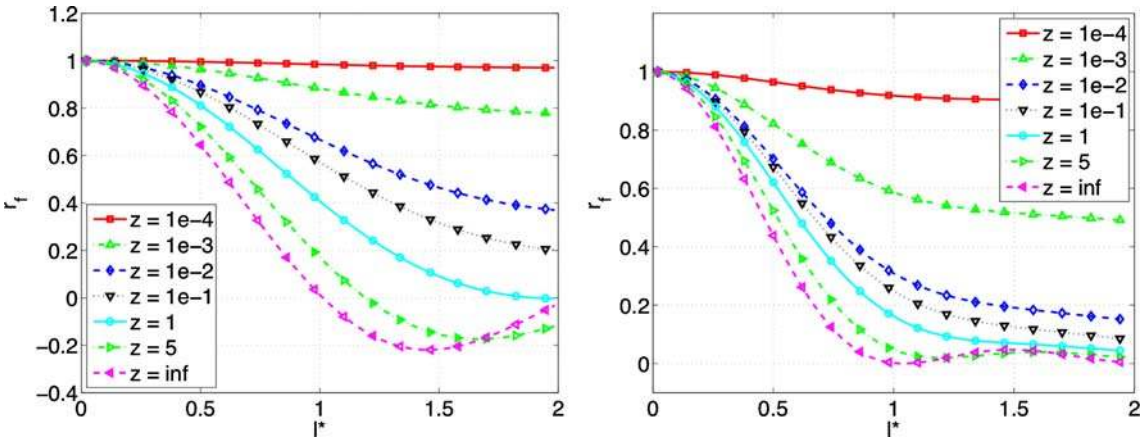

Fig. 6 Convolution filter spatial response, one-dimensional (*left*) and two-dimensional (*right*)

3.5 Theoretical stability analysis

To indicate the stability of the process, the ratio between consecutive updates is used. Similarly to what is proposed by Nogueira et al. (1999), the expression for the stability coefficient ε with respect to a generic velocity vector component u reads as:

$$\varepsilon \equiv \frac{u^{k+1} - u^k}{u^k - u^{k-1}}. \tag{11}$$

when $0 \leq \varepsilon < 1$ the ratio of updates is monotonically decreasing ensuring a stable process. If $-1 < \varepsilon < 0$ the process is still stable, however sign reversal occurs in the value of the updates (oscillations of decreasing amplitude). r_f and r_c can be obtained from previous definitions considering that $r_c = \text{sinc}(l^*)$ and $r_f = f(l^*)$ (see Fig. 6). The stability of the process therefore depends only on the value of l^* and on the properties of r_f, which again are determined by the parameter z.

In the case of predictor filtering the stability criterion can be derived combining Eqs. (5) and (11):

$$\varepsilon = r_f \cdot (1 - r_c). \tag{12}$$

The behaviour of the stability coefficient in case of predictor filtering is shown in Fig. 7 for a one-dimensional signal and in Fig. 8 for a two-dimensional one.

For normalized wavelengths smaller than 1 ($l^* < 1$) all filters are expected to be stable. When applying top-hat filtering ($z = \infty$) the instability parameter varies from positive to negative values. Decreasing the values of z the parameter ε increases indicating that the process becomes less stable. When z is decreased from 10^{-2} to 10^{-3} the process goes from stable to unstable for signals containing wavelengths smaller than the window size ($l^* > 1$). Eventually this means that the presence of noise which minimum wavelength ultimately only depends on the vector spacing will destabilize the process.

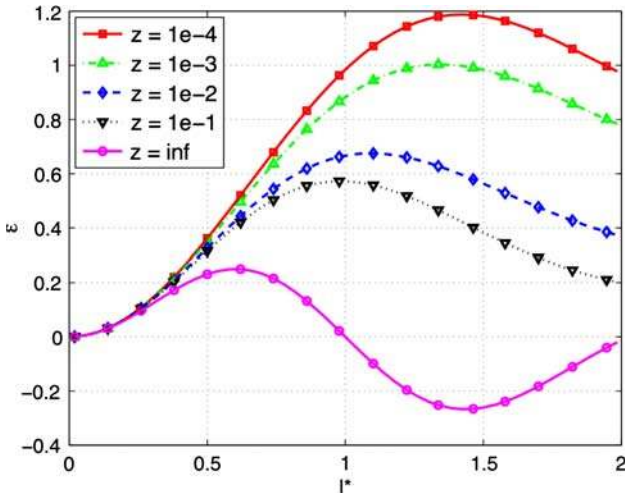

Fig. 7 Stability coefficient as a function of the normalized window size l^* for different values of the predictor filter strength for the one-dimensional case

The dependence of the stability coefficient on the filter parameter z for the two-dimensional case is similar to the one-dimensional case, except for the fact that $0 \leq \varepsilon \leq 1$ for all choices of the parameter z. This indicates that for two-dimensional waves with equal wavelengths in x and y direction, the process is expected to be always stable irrespective of the wavelength.

The parameter ε yields not only information on the stability of the process; it also indicates the rate of convergence. The smaller the absolute value of ε the faster the process converges. Therefore the fastest convergence is expected for the top-hat filter.

The stability criterion for corrector filtering can be obtained combining Eqs. (7) and (11):

$$\varepsilon = (1 - r_f \cdot r_c). \tag{13}$$

This is graphically represented in Fig. 9 for a one-dimensional signal and in Fig. 10 for a two-dimensional one.

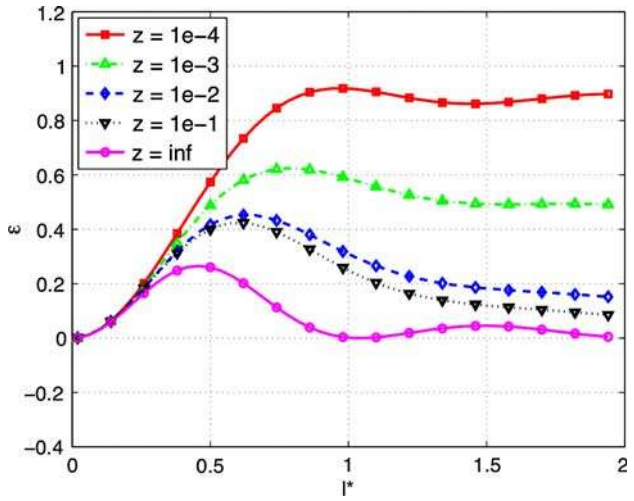

Fig. 8 Stability coefficient as a function of the normalized window size l^* for different values of the predictor filter strength for the two-dimensional case

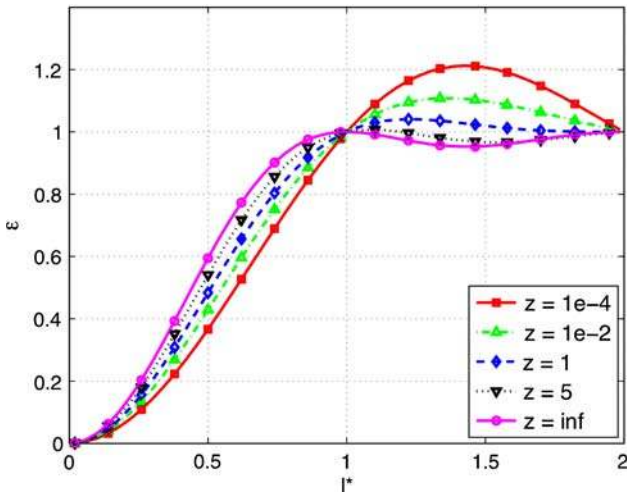

Fig. 9 Stability coefficient as a function of the normalized window size l^* for different values of the corrector filter strength z for the one-dimensional case

From Fig. 9 it can be seen that, similar to the predictor case, when $l^* < 1$ (wavelengths larger than the window size) the process is stable for all filters because $0 \leq \varepsilon \leq 1$. At $l^* = 1$ the spatial response of the cross correlation process is $r_c = 0$, therefore $\varepsilon = 1$ irrespective of the corrector filter strength (see Eq.13). For wavelengths smaller than the window size, $l^* > 1$, all filters are found to be unstable except for the top-hat filter.

However, anticipating the numerical results, for $z > 1$ the susceptibility to destabilization is expected to be small since the corrector filtering approach only acts indirectly on the final result.

In case of the purely two-dimensional signal the stability coefficient is $0 \leq \varepsilon \leq 1$, which is similar to the

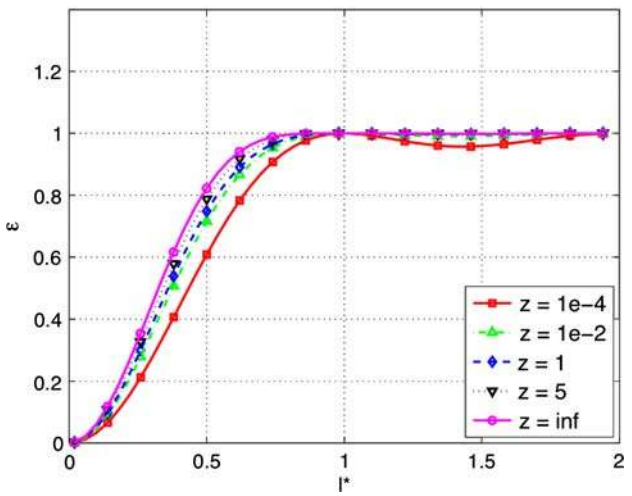

Fig. 10 Stability coefficient as a function of the normalized window size l* for different values of the corrector filter strength z for the two-dimensional case

two-dimensional predictor filtering, showing that also in this case there are no stability issues for two-dimensional waves with similar wavelengths along x and y direction.

When comparing the stability coefficient for the predictor and corrector filtering it can be inferred that the convergence rate (the inverse of the stability coefficient) in case of corrector filtering is always lower compared to predictor filtering.

3.6 Spatial resolution

In the following section the spatial resolution of the iterative process is studied by analysing the modulation effect. Considering the stable range, $l^* < 1$, the iterative equation can be rewritten with the asymptotic limit that $\lim_{k\to\infty}\left(u^{k+1} - u^k\right) = 0$ to obtain the asymptotic amplitude response.

Introducing the limit into Eq. (5) results in the asymptotic amplitude response for predictor filtering:

$$\frac{u^\infty}{u_0} = \frac{r_c}{1 - r_f + r_c \cdot r_f}. \tag{14}$$

In the limit case that $r_f \to 1$ ($z \to 0$), $u^\infty/u_0 \to 1$ is obtained, i.e. no modulation. Although this behaviour would yield the highest spatial response, the above discussion on stability excludes this possibility. When $r_c \to 1$ ($l^* \to 0$, the wavelength is large compared to the window size), the modulation effect vanishes and the velocity fluctuation amplitude tends to the exact value.

The amplitude modulation increases with the parameter z (Figs. 11, 12). However, it is remarkable that even the response for $z \to \infty$ is significantly less modulated with respect to a moving average filter. This behaviour is due to the iterative implementation of the interrogation process.

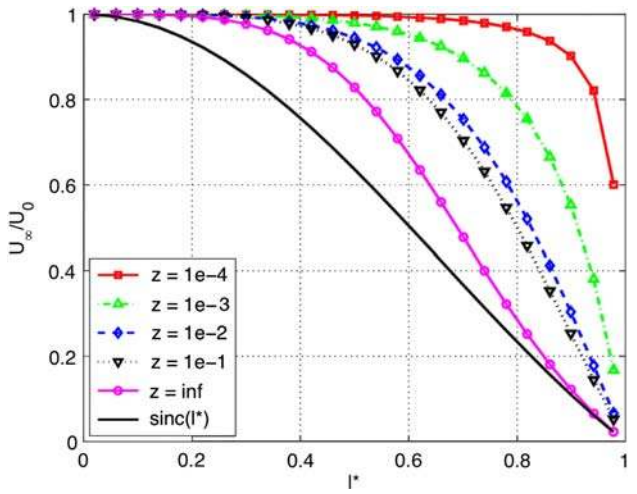

Fig. 11 Predictor filtering asymptotic amplitude response for the one-dimensional case

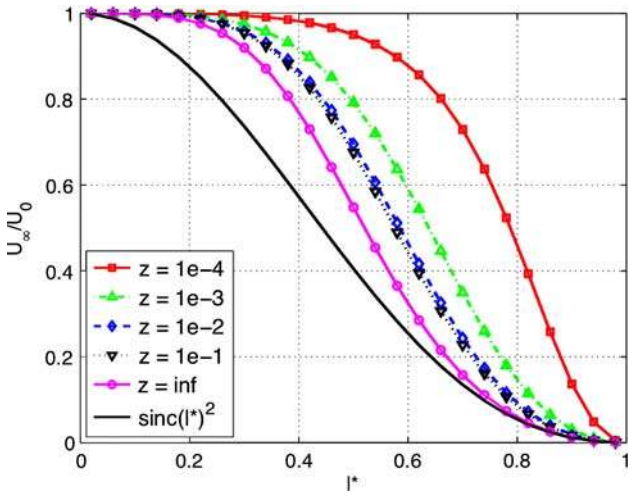

Fig. 12 Predictor filtering asymptotic amplitude response for the two-dimensional case

Which makes the window deformation approach advantageous with respect to the window shift technique, which behaves as a moving average filter (Scarano and Riethmuller 2000a). For example, in case of a one-dimensional signal the -3 dB cut-off value ($u^{\infty}/u_0 = 0.5$) is shifted from $l^* = 0.6$ for a single pass method to $l^* = 0.7$ for the iterative process at $z = \infty$ and to $l^* = 0.83$ for the iterative process at $z = 10^{-2}$. Furthermore, it can be seen that the improvement due to the iterative implementation of the interrogation process in terms of amplitude modulation is especially large for small l^*. Similar conclusions can also be drawn for the two-dimensional signal case.

Using the above analysis it is now possible to select an appropriate value for the parameter z such to optimize the filtering process. This can be further illustrated by observing that the modulation decreases when decreasing z therefore a value of z as low as possible is desired. However, when $z \leq 10^{-3}$ the process is found to be unstable for certain wavelengths (see Sect. 3.5), eventually causing the process to become unstable independently of the signal wavelength, due to the presence of high frequency noise. Therefore $z = 10^{-2}$ seems close to an optimum: it offers a stable process, with a good rate of convergence and high spatial response. In the rest of the discussions this value of $z = 10^{-2}$ will be referred to as the critical z for predictor filtering or $z_{c,p}$. It should be remarked here that the choice of the filter shape is not unique and similar behaviour may have been achieved with a different base function for the filter. However, the main conclusion is that when z is smaller than a given value the effective filter width is below the necessary value to damp unstable wavelengths.

In case of the corrector filtering process (Eq. 7) the limit assumption results in an asymptotic amplitude response, which is identical to one for all wavelengths and irrespective of the filter strength:

$$\frac{u^{\infty}}{u_0} = 1. \tag{15}$$

This means that theoretically the corrector filtering process does not suffer from modulation effects. Although this behaviour may seem strange at first, it can be understood when realizing that only the update (corrector) is filtered. This means that the error caused by the modulation is corrected in the next step of the iterative process, where the update is again subjected to filtering. In this way the process asymptotically converges to the non-modulated value.

However, when increasing the corrector filter strength z the convergence rate decreases, therefore the smallest possible value for z should be chosen. As in the predictor filtering case a lower bound concerning the z parameter should be given by the stability analysis. However, it was found that all filter strengths resulted in an unstable process. As also mentioned in Sect. 3.5, the susceptibility to destabilization can be neglected for $z \geq 1$, therefore $z_{c,c} = 1$ is proposed as the critical z for corrector filtering. The choice for this value is justified in the numerical assessment.

4 Numerical assessment

A theoretical analysis based on linear filtering analogy has been performed in Sect. 3 in the hypothesis that the cross-correlation interrogation yields the noise-free local average of the particle displacement over the window.

A numerical assessment is presented in this section, where computer generated PIV recordings are processed with known image and displacement properties. In this way the linear filter hypothesis can be removed. Moreover

one-dimensional as well as two-dimensional cases will be considered. The particle images are generated using Monte Carlo simulation. The mean particle image size is $d_p = 2.5$ pixels with a standard deviation of 0.2 pixels. The particle image density is 0.1 particles per pixel, which yields approximately 100 particles within a window of 31×31 pixels. The mean particle peak intensity is 2,000 with a standard deviation of 300 counts. Two displacement fields are used in the assessment: a one-dimensional sinusoidal shearing motion with a varying wavelength from 620 to 30 pixels and a two-dimensional sinusoidal displacement resulting in a vortex-like flow-field covering the same wavelength range as in the one-dimensional case. The equation for the two-dimensional case reads:

$$\begin{aligned} u(x,y) &= U_0 \sin(2\pi x/\lambda)\sin(2\pi y/\lambda) \\ v(x,y) &= V_0 \cos(2\pi x/\lambda)\cos(2\pi y/\lambda) \end{aligned}. \tag{16}$$

The maximum particle displacement is equal to 1 pixel ($U_0 = V_0 = 1$) in the one-dimensional and the two-dimensional cases. The images are analysed with the WIDIM algorithm (Scarano and Riethmuller 2000a) with the modification that the filter parameter z (Eq. 9) can be varied. The interrogation window size is 31×31 pixels and an overlap factor of 90% is chosen to minimize the error due to spatial discretization. The correlation results are again linearly interpolated onto a pixel grid on which the filter is applied to further reduce discretization effects. Similar to the theoretical assessment, the filter window size has been chosen equal to that of the PIV image interrogation window. With the current settings the numerical assessment covers a normalized wavelength range from 0.05 to 1.0 since this is the specific area of interest for PIV interrogation algorithms.

The results are given in terms of amplitude modulation and root mean square (rms) fluctuations. The modulation is obtained by calculating the area under a half-sinusoid wave obtained by the interrogation process and comparing this to the area under an exact half-sinusoid wave. For a one-dimensional signal this can be mathematically represented by:

$$\frac{U}{U_0}(l^*) = \frac{\int_0^{\lambda/2} U(l^*,x)dx}{\lambda U_0/\pi}, \tag{17}$$

where U is the displacement obtained from the interrogation process, U_0 is the actual maximum displacement amplitude and λ is the signal wavelength under consideration.

The rms error is obtained from the interrogation process result. The rms is determined at each location in a wave (by using multiple realizations) and is averaged over a complete wavelength. In case of a one-dimensional signal the expression is given by:

$$\mathrm{rms}(l^*) = \frac{1}{K}\sum_{k=1}^{K}\left[\frac{\sum_{n=1}^{N}\left[u(l^*,k,n) - \overline{u}(l^*,k)\right]}{N}\right]^{\frac{1}{2}}. \tag{18}$$

where n is the wave realization number with N total realizations, k is the integer position on the vector grid in the wave and K is the integer wavelength. K and k are linked to the spatial position x and wavelength λ by:

$$x = \lambda\left(\frac{k-1}{K-1}\right). \tag{19}$$

4.1 Predictor filtering

4.1.1 *One-dimensional sinusoidal displacement with varying wavelength*

Figure 13 illustrates the development of the spatial response after several iterations. The iterative process appears to be stable for $z \geq z_{c,p}$ ($z_{c,p} = 10^{-2}$). It converges very slowly for $z = 10^{-3}$ and is overshooting for $z = 10^{-4}$ ($U/U_0 > 1$ at iter = 10). For $z < z_{c,p}$ and $l^* < 0.5$ the modulation gain is small when decreasing the filter strength. The expected gain in terms of spatial resolution going from the top-hat case ($z \to \infty$) to the critical case

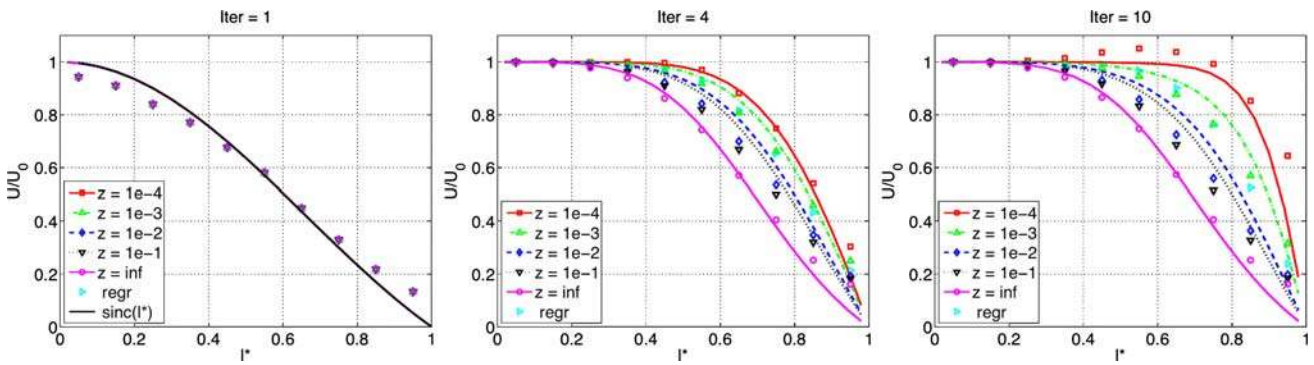

Fig. 13 Spatial response of cross-correlation analysis for a one-dimensional sinusoidal displacement as a function of the normalised window size l^* and for different values of the predictor filter parameter z (*solid lines* are the corresponding theoretical curves)

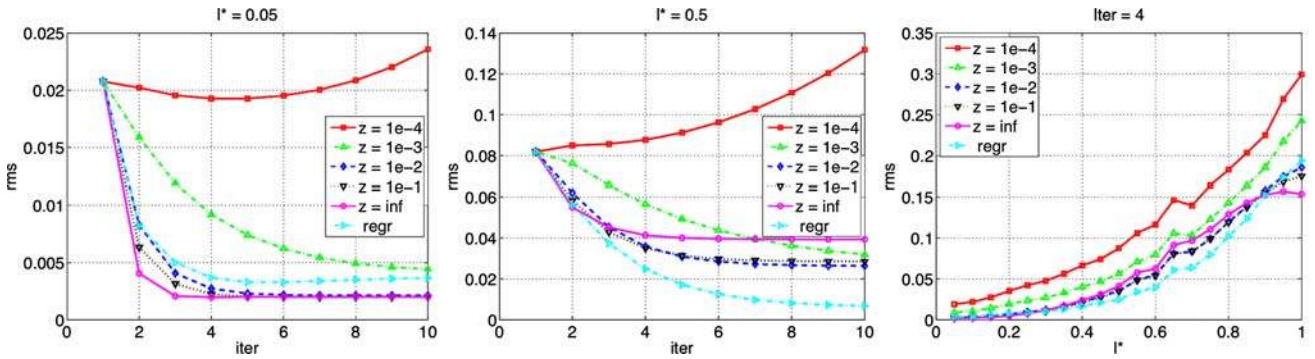

Fig. 14 RMS error of cross-correlation analysis for a one-dimensional sinusoidal displacement as a function of the number of iterations and predictor filter parameter (*left* and *centre*) or as a function of the normalized window size l^* and predictor filter parameter z (*right*)

$z = z_{c,p}$ is in qualitative agreement with the theoretical prediction. Assessing the non-linear regression filter it can be seen that it performs similar to the $z = 10^{-3}$ linear filter. The variation of rms error with increasing iteration number is given in Fig. 14 left and middle, which is a good indicator for the stability of the process. At $l^* = 0.05$ the rms error is constant for $z > z_{c,p}$, converges slowly for $z = z_{c,p}$ and diverges for the case $z \to 0$. Although all filters are stable at this wavelength according to Fig. 7, high frequency fluctuations (due to noise by for example round off errors) cause the unstable behaviour present for $z < z_{c,p}$ (see Sect. 3.5). At $l^* = 0.5$ the situation is less pronounced as for $l^* = 0.05$, this is because of the increased modulation. However, when $z = 10^{-4}$ the process is still unstable. In Fig. 14 right, the rms error is given as function of l^* at the 4th iteration. It can be observed that the rms error increases with l^* and decreases with increasing filter strength. Finally it is found that the non-linear regression filter generally has a lower rms error as expected, Fig 15.

4.1.2 *Two-dimensional sinusoidal displacement with varying wavelength*

The results obtained from the two-dimensional displacement field are similar to the one-dimensional case except for the fact that the slope of all curves tends to zero towards $l^* = 1$. Decreasing the parameter z, also decreases the modulation. For $l^* < 0.2$ the modulation is independent of the filter parameter. Looking at the rms as a function of the iteration number (Fig. 16 left and middle), the situation is exactly the same as in the one-dimensional case. When observing the rms values for $l^* < 1$ at iteration 4 (Fig. 16 right) it is seen that for $z \geq z_{c,p}$, the rms error does not depend on the filter parameter. For $z < z_{c,p}$ the rms increases with decreasing z. Finally, for the two-dimensional case it was found that the regression filter is comparable with the $z = 10^{-2}$ filter and also exhibits overall low rms values.

This confirms that the filter with $z = 10^{-4}$ is unstable. For $z = 10^{-3}$ the behaviour of the rms with increasing iterations shows that the filter is marginally stable since only a slow convergence is found. At $z = 10^{-2}$ the filter is found to be stable. This confirms the theoretical analysis.

Table 1 shows the value of l where the measured displacement drops below the -3 dB point for the total error. In this case the total error is computed as the Euclidean norm of the modulation and rms effects. It should be retained in mind that the total error also contains a component that is a function of the wave amplitude (which is 1 pixel in this assessment). It is however useful to combine

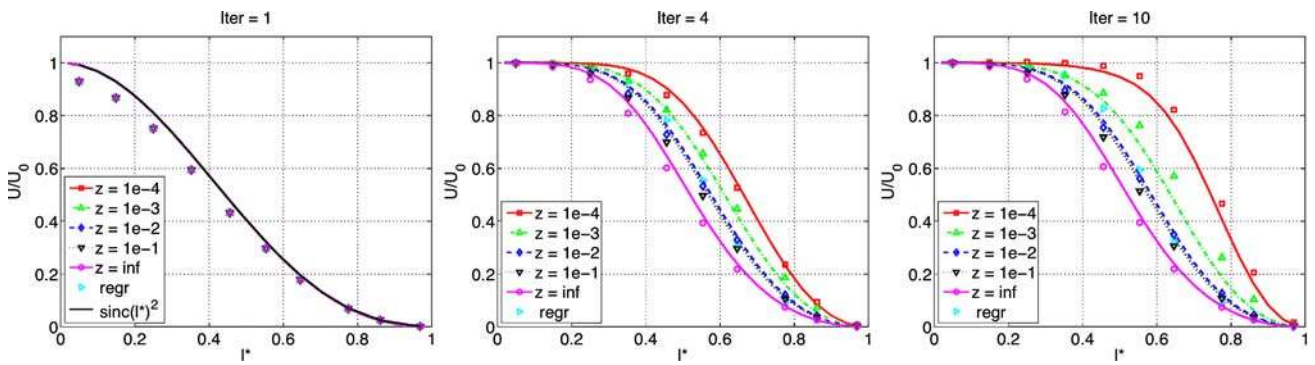

Fig. 15 Spatial response of cross-correlation analysis for a two-dimensional sinusoidal displacement as a function of the normalised window size l^* and for different values of the predictor filter parameter z (*solid lines* are the corresponding theoretical curves)

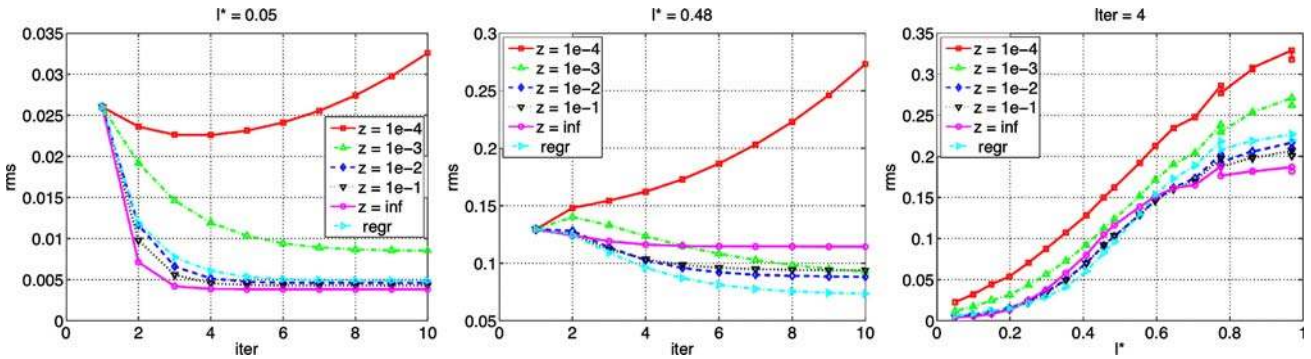

Fig. 16 RMS error of cross-correlation analysis for a two-dimensional sinusoidal displacement as a function of the number of iterations and predictor filter parameter (*left* and *centre*) or as a function of the normalized window size l^* and predictor filter parameter z (*right*)

Table 1 Normalized window size l^* at −3 dB total error cut-off point for predictor filtering (after four iterations)

l^*	$z = 10^{-4}$	$z = 10^{-3}$	$z = 10^{-2}$	$z = 10^{-1}$	$z = \infty$	regr	sinc
One-dimensional	0.79	0.77	0.72	0.70	0.64	0.78	0.60
Two-dimensional	0.57	0.55	0.51	0.50	0.45	0.53	0.44

both components of the error for sake of compactness. The one-dimensional and two-dimensional signals give similar results; only the cut-off normalized window size is reduced for the two-dimensional case, which is expected. Overall it is found that the cut-off point is increased (higher l^*) with decreasing filter strength. The regression filter is found to yield the same cut-off point as the predictor filter with $z = 10^{-3}$, which, however is marginally stable. Finally the cut-off point for the sinc function is included which corresponds to the single-pass or window-shift interrogation processing, clearly showing the benefits of iterative processing.

4.2 Corrector filtering

4.2.1 *One-dimensional sinusoidal displacement with varying wavelength*

The spatial response of the corrector filtering process is given in Fig. 17. Looking at the theoretical curves (solid lines) it can be seen that as the iterations progress the modulation decreases. When comparing this to the numerical assessment (symbols), it is found that this holds for filter strength $z > 5$. For weaker filter strengths, the process overshoots when increasing with iterations. The extent of the overshoot however decreases with increasing filter strength. Observing the evolution of the rms values with iteration number (Fig. 18 left and middle) shows that for $z < z_{c,c}$ the process diverges.

At iteration 4 (Fig. 18 right) the rms error increases with l^*. For a given l^* the rms decreases with the filter strength, this decrease is rather strong for $z < z_{c,c}$ and becomes weaker for $z > z_{c,c}$. Overall the situation is similar to the predictor filtering case, Fig. 19.

4.2.2 *Two-dimensional sinusoidal displacement with varying wavelength*

For $l^* < 0.2$ the modulation is found to be independent of the filter parameter z. The modulation decreases with the filter strength z and a minimal overshoot is found for $z = 10^{-4}$. From Fig. 20 left and middle, it can be seen that the filters with $z < z_{c,c}$ show an increase of rms error with iteration, for $z \geq z_{c,c}$ the rms values are found to decrease with the iteration number. The increase in rms with l^* at iteration 4 (Fig. 20 right) is similar to the one-dimensional case. For $z \geq z_{c,c}$ the rms is very weakly dependent on the filter strength (almost constant) while it strongly increases for decreasing z when $z < z_{c,c}$. The above observations concerning the modulation are found to be consistent with the theoretical analysis. The rms error diagrams showed that the process is stable for $z = 1$ and unstable for $z = 10^{-2}$.

Finally the −3 dB total error criterion is summarized in Table 2. As in the predictor filtering case, the cut-off point increases with decreasing filter strength z. Again the increase in cut-off point is found when going from one-step (sinc) to iterative processing.

When comparing the cut-off point obtained from predictor to corrector filtering it is found that the corrector filter yield the best results. This can be attributed to the better modulation response, however one should keep in

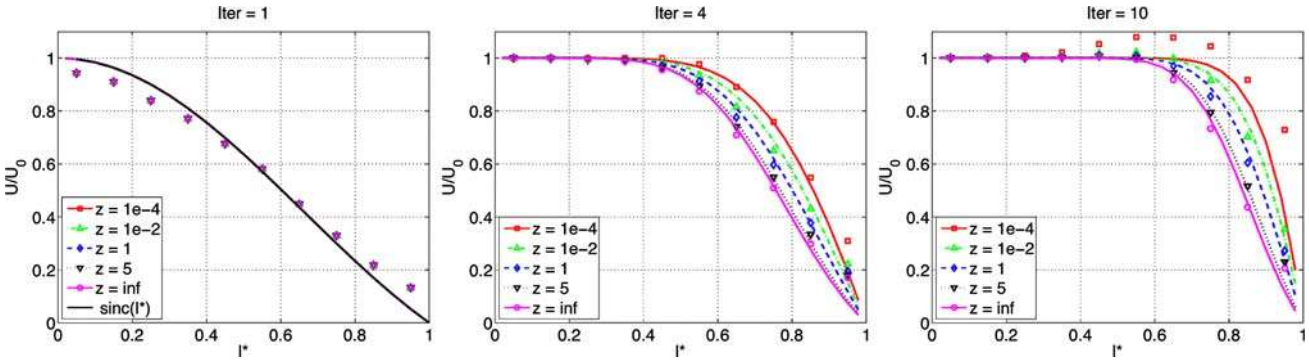

Fig. 17 Spatial response of cross-correlation analysis for a one-dimensional sinusoidal displacement as a function of the normalized window size l^* and for different values of the corrector filter parameter z (*solid lines* are the corresponding theoretical curves)

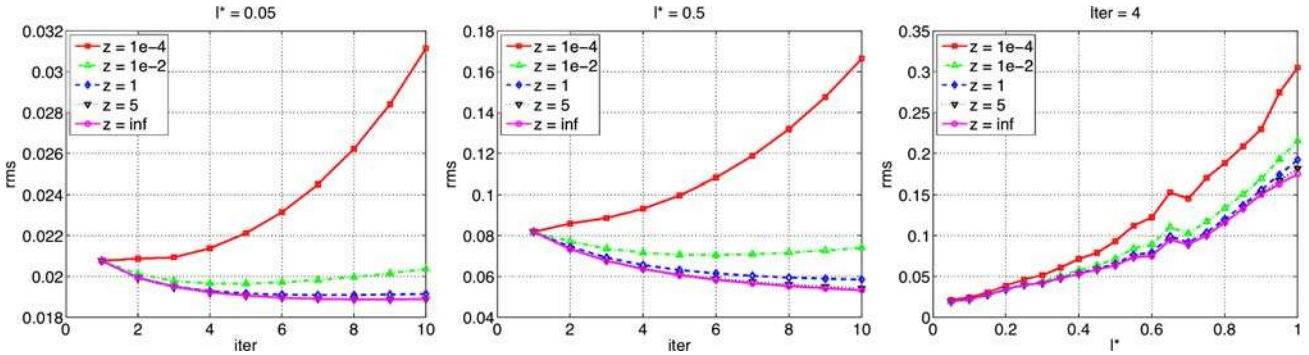

Fig. 18 RMS error of cross-correlation analysis for a one-dimensional sinusoidal displacement as a function of the number of iterations and corrector filter parameter (*left* and *centre*) or as a function of the normalized window size l^* and corrector filter parameter z (*right*)

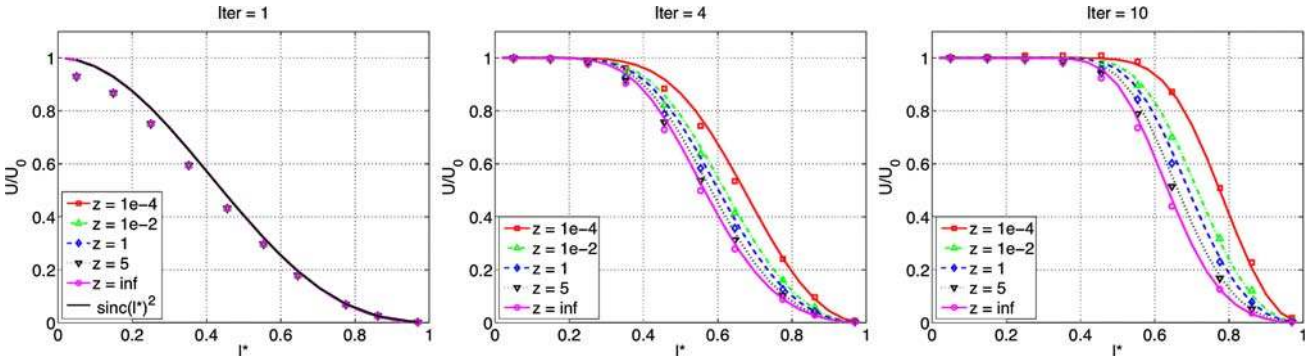

Fig. 19 Spatial response of cross-correlation analysis for a two-dimensional sinusoidal displacement as a function of the normalised window size l^* and for different values of the corrector filter parameter z (*solid lines* are the corresponding theoretical curves)

mind that the rms values are generally larger for the corrector filter and that it is more susceptible to instabilities.

5 Experimental assessment

To assess the filtering approaches under real experimental conditions, PIV images of the water flow over a backward facing step are used (Scarano and Riethmuller 2000b). The flow facility is a gravity driven closed circuit water tunnel. The inlet channel has a 100 × 240 ($h \times w$) mm^2 cross-section before expansion. The backward facing step height is $h = 20$ mm and the expansion ratio is 1.2. A double cavity pulsed Nd:Yag laser ($\sim$120 mJ/pulse) was used as light source. LATEX particles (dp $\sim$25 μm) are used as seeding. An example of the flow field is given in Fig. 21.

The scattered light was acquired by means of a PCO sensicam CCD camera having 1,280 × 1,024 pixels (12 bits) which was cropped to 1,280 × 320 pixels. The time separation between the laser pulses was $\Delta t = 5$ ms.

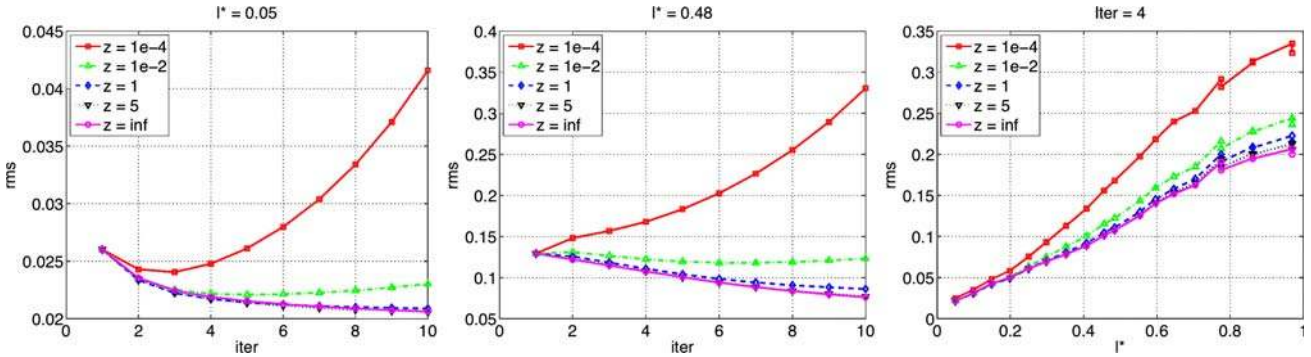

Fig. 20 RMS error of cross-correlation analysis for a two-dimensional sinusoidal displacement as a function of the number of iterations and corrector filter parameter (*left* and *centre*) or as a function of the normalized window size l^* and predictor filter parameter z (*right*)

Table 2 Normalized window size l^* at −3dB total error cut-off point for corrector filtering (after four iterations)

l^*	$z = 10^{-4}$	$z = 10^{-2}$	$z = 1$	$z = 5$	$z = \infty$	sinc
One-dimensional	0.79	0.76	0.75	0.73	0.71	0.60
Two-dimensional	0.57	0.55	0.53	0.52	0.50	0.44

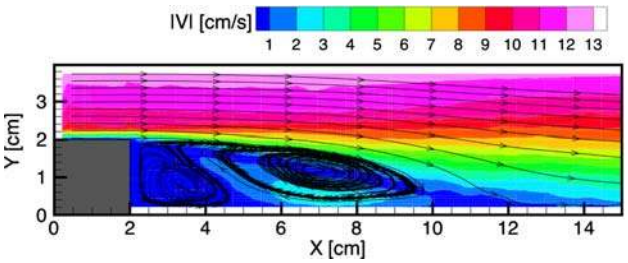

Fig. 21 Averaged PIV result for the flow over the backward facing step

Experiments were conducted at $Re_h = 5.0 \times 10^3$, with a free-stream velocity of $U_\infty = 12.5$ cm s^{-1}. The overall field of view is 160 × 40 mm^2 (magnification is 0.054). For the statistical analysis 200 images were used. The interrogation window size was set to 31 × 31 pixels with an overlap factor of 80%.

In Fig. 22, the results for the different filtering approaches are reported, the scales are equal to Fig. 21.

The comparison of the results shows little difference between the different choices (predictor or corrector filter, values of z), except for a clearly diminished resolution due to excessive filtering when the top-hat filter is applied to the predictor (Fig. 22 topright where for example the local velocity maximum is modulated in the recirculation zone behind the step). Conversely, the unfiltered analysis (Fig. 22 topleft) shows an increased noise.

In Figs. 23 and 24, respectively the horizontal and vertical velocity components are given on a line that crosses the shear layer at $x = 2.5$ cm. These figures clearly show the increased modulation for the moving average predictor filter. They also show the instability for the non-filtered (local) process resulting in the amplification of initial disturbances resulting in a wavy pattern around the expected shear layer profile (Fig. 23).

Finally in Figs. 25 and 26, the rms values of the vertical velocity component at respectively $y = 3$ and $x = 10$ cm are shown. Except for the local and the moving average predictor filter (pz∞) all methods return similar rms values. In case of the local method the rms values are increased due to the unstable nature of the method. On the other hand when using the moving average predictor, the rms values are attenuated because of excessive smoothing. In Table 3 this is also expressed as the mean rms value over the profiles given in Figs. 25 and 26. Here it can be seen that the local method gives a 10% increase in rms values while the moving average predictor results in a 5% attenuation of the rms fluctuations.

6 Conclusions

The stability and resolution of iterative PIV image analysis with spatial filtering methods have been investigated theoretically by means of linear filter analogy, subsequently a numerical and experimental assessment was performed. The numerical study focuses on sinusoidal one-dimensional waves representing flow fields where a wavelength dominates in one direction (shear layers, shock waves) and purely two-dimensional waves where the wavelength is equal in all directions (isotropic turbulence, vortices). The discussion shows that for iterative image deformation methods without image weighting and overlap factors higher than 50% it is essential to introduce a low-pass filter within the iterative cycle to avoid the amplification of unstable wavelengths. A family of filters has been introduced of a form that the filter shape could be varied with a single parameter and covering the two opposite cases of

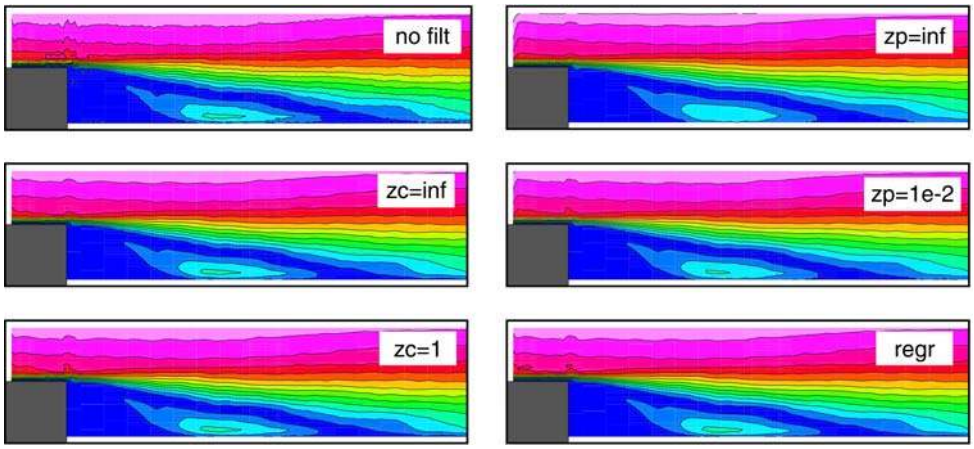

Fig. 22 Analysis of PIV recordings with different filtering approaches. Mean velocity magnitude over 200 recordings after four iterations, *scale* is the same as in Fig. 21

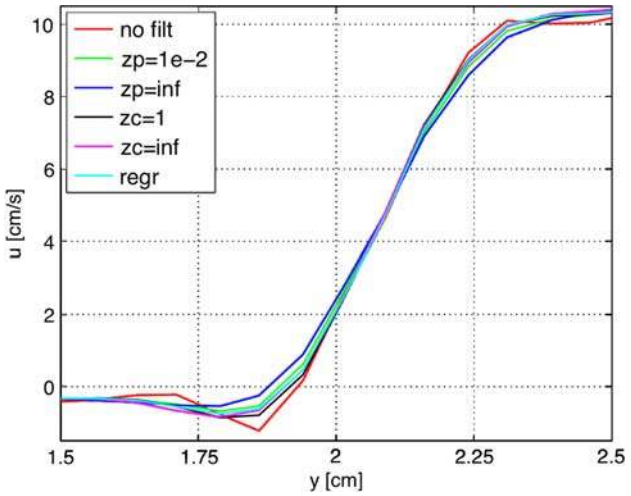

Fig. 23 Average horizontal velocity component on the line $x = 2.5$ cm

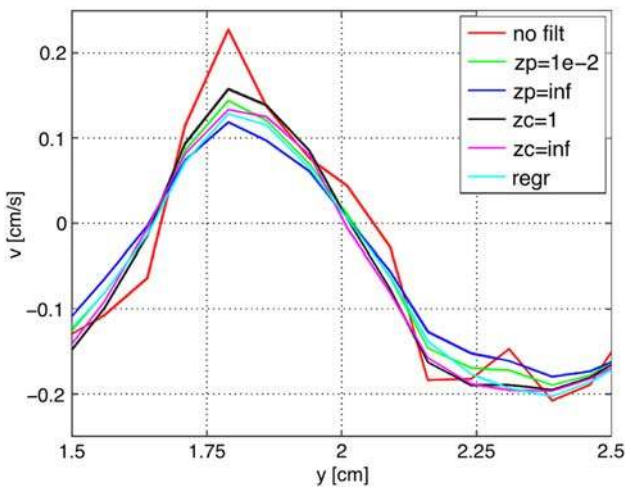

Fig. 24 Average vertical velocity component on the line $x = 2.5$ cm

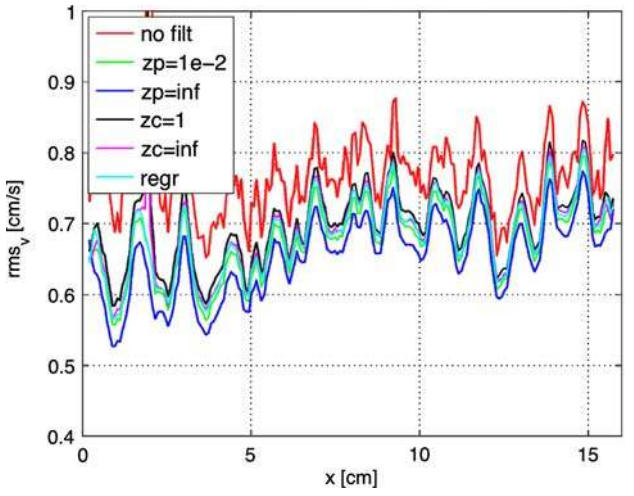

Fig. 25 Rms of the vertical velocity component on the line $y = 3$ cm

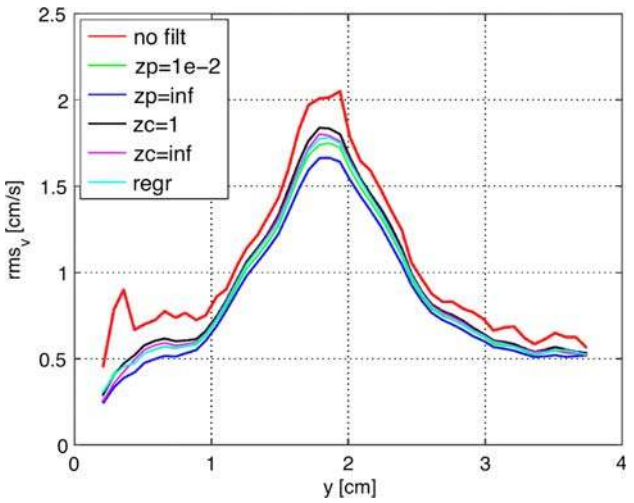

Fig. 26 Rms of the vertical velocity component on the line $x = 10$ cm

Dirac pulse and top-hat filter shape. The filter size was chosen to be equal to the PIV interrogation window size. Two filtering approaches were studied; predictor filtering where the filter acts on the measured displacement and corrector filtering where the filter is applied to the update term. The filter and interrogation window size used in the

Table 3 Mean rms values of the graphs given in Figs. 25 and 26

	No filt	zp = 1e − 2	zp = inf	zc = 1	zc = inf	regr
$x = 5$ cm	1.03	0.88	0.84	0.91	0.90	0.89
$y = 3$ cm	0.77	0.68	0.65	0.70	0.69	0.68

investigation was 31 × 31 pixels. Finally also a non-linear filter was introduced in the predictor filtering approach.

The main result from the theoretical discussion and numerical assessment is a critical value (minimum) for the filter parameter: for predictor filtering below $z = 10^{-2}$ poor convergence is to be expected and for lower values the process is unstable. The critical value for corrector filtering is found to be $z = 1$. The spatial resolution depends less strongly on the filter parameter, however one result stands clear: an important gain in the −3 dB cut-off frequency is obtained going from a single-pass interrogation to the iterative interrogation.

The corrector filtering strategy was found to yield an appreciably better spatial resolution with respect to the predictor filtering, however at the cost of higher rms values and lower convergence rate. The regression filter showed good modulation characteristics, combined with low rms values.

The experimental assessment confirmed the theoretical prediction and numerical assessment. The analysis of the PIV recordings of the flow over a backward facing step clearly documents the effects of noise amplification in case of insufficient or disabled predictor filtering as well as attenuation effects caused by excessive filtering. It was found that the measured rms fluctuations were overpredicted by 10% for unstable processes while for excessive filtering the rms fluctuations were decreased by 5%.

Acknowledgments This work is supported by the Dutch Technology Foundation STW under the VIDI program grant DLR.6198.

References

Astarita T (2006) Analysis of interpolation schemes for image deformation methods in PIV: effect of noise on the accuracy and spatial resolution. Exp Fluids 40:977–987

Astarita T (2007) Analysis of weighting windows for image deformation methods in PIV. Exp Fluids 43:859–872

Astarita T, Cardone G (2005) Analysis of interpolation schemes for image deformation methods in PIV. Exp Fluids 38:233–243

Fincham A, Delerce G (2000) Advanced optimization of correlation imaging velocimetry algorithms. Exp Fluids 22(7): S13–S22

Huang HT, Fielder HF, Wang JJ (1993) Limitation and improvement of PIV, part II. particle image distortion. a novel technique. Exp Fluids 15:263–273

Jambunathan K, Ju XY, Dobbins BN, Ashforth-Frost S (1995) An improved cross correlation technique for particle image velocimetry. Meas Sci Technol 6:507–514

Keane RD, Adrian RJ (1993) Theory of cross-correlation analysis of PIV images, flow visualization and image analysis. In: Nieuwstadt FTM (ed) Kluwer, Dordrecht, pp 1–25

Lecordier B (1997) Etude de l'interaction de la propagation d'une flamme premelangee avec le champ aerodynamique, par association de la tomographie Laser et de la Velocimetrie par Images de particules. These de doctorat de l'Universite de Rouen, Rouen, France

Lecordier B, Trinité M (2003) Advanced PIV algorithms with image distortion—validation and comparison from synthetic images of turbulent flow. 5th international symposium on particle image velocimetry, Busan, Korea

Nogueira J, Lecuona A, Rodriguez PA (1999) Local field correction PIV: on the increase of accuracy of digital PIV systems. Exp Fluids 27:107–116

Nogueira J, Lecuona A, Rodriguez PA (2001) Local field correction PIV, implemented by means of simple algorithms, and multigrid versions. Meas Sci Technol 12:1911–1921

Nogueira J, Lecuona A, Rodriguez PA (2005) Limits on the resolution of correlation PIV iterative methods. Fundamentals. Exp Fluids 39:305–313

Scarano F (2004) On the stability of iterative PIV image interrogation methods, 12th international symposium on applications of laser techniques to fluid mechanics. Lisbon, Portugal

Scarano F, Riethmuller ML (1999) Iterative Multigrid approach in PIV image processing with discrete window offset. Exp Fluids 26:513–523

Scarano F, Riethmuller ML (2000a) Advances in iterative multigrid PIV image processing. Exp Fluids 29(7): S51–S60

Scarano F, Riethmuller ML (2000b) Temporal analysis of coherent structures in a turbulent BFS flow with PIV. 10th international symposium on applications of laser techniques to fluid mechanics. Lisbon, Portugal

Scarano F, Schrijer FFJ (2005), Effect of predictor filtering on the stability and spatial resolution of iterative PIV interrogation. 6th international symposium on particle image velocimetry, Pasadena, California, USA

Schrijer FFJ, Scarano F (2006) On the stabilization and spatial resolution of iterative PIV interrogation. 13th international symposium on applications of laser techniques to fluid mechanics, Lisbon, Portugal

Soria J (1996) An investigation of the near wake of a circular cylinder using a video-based digital cross-correlation particle image velocimetry technique. Exp Therm Fluid Sci 12:221–233

Stanislas M, Okamoto K, Kähler CJ, Westerweel J (2005) Main results of the second international PIV challenge. Exp Fluids 39:170–191

Westerweel J, Dabiri D, Gharib M (1997) The effect of a discrete window offset on the accuracy of cross-correlation analysis of digital PIV recordings. Exp Fluids 23:20–28